DISCLAIMER NOTICE

THIS DOCUMENT IS BEST QUALITY PRACTICABLE. THE COPY FURNISHED TO DTIC CONTAINED A SIGNIFICANT NUMBER OF PAGES WHICH DO NOT REPRODUCE LEGIBLY.

63-1-2

RENSSELAER POLYTECHNIC INSTITUTE
Department of Geology

Technical Report No. 4

Stress Propagation in Non-linear Viscoelastic Materials: Unloading Cycle

Edward J. Mercado*

September 14, 1962

Prepared for:

Ballistic Research Laboratories

Aberdeen Proving Ground, Maryland

Technical Monitors

B. Perkins
A. A. Thompson

Contract No. DA-30-115-509-ORD-1009

Approved:

Samuel Katz

Samuel Katz
Project Supervisor

*Now at Gulf Research and Development Co., Pittsburgh, Pa.

ABSTRACT

Stress propagation in a nonlinear viscoelastic material is analyzed for the unloading portion of a complete stress-strain cycle. The loading process is the subject of a previous report. The elastic unloading theory developed by Malvern is reviewed and extended to include stress-strain laws with nonlinear unloading. Numerical techniques for solution are outlined for both infinitesimal and finite strain theories.

LIST OF SYMBOLS

σ - stress

V - particle velocity

ε - infinitesimal strain or space gradient of displacement

α - finite strain = $\varepsilon + \frac{1}{2}\varepsilon^2$

E - Young's modulus

a, b - dynamic constants of material

ρ - density

C - velocity of initial wave front

t - time

x - Lagrangian space variable

All other terms are defined in the text where first introduced.

INTRODUCTION

Experimental evidence from the dynamic testing of metals and earth materials indicates that upon removal of external forces exceeding the yield point, the material does not return to its initial state. A commonly accepted procedure for dealing with this hysteresis effect is to assume that the stress-strain laws in the loading and unloading cycles are not the same. The material is often assumed to unload elastically with slope equal to that of the initial elastic loading path. Boundary value problems associated with materials that behave plastically on loading and elastically on unloading have been discussed by Lee.[1] Materials that behave plastically on both loading and unloading have been investigated by Morland.[2] Unloading phenomena in strain-rate sensitive materials have been investigated by Malvern[3] with a subsequent contribution by Rubin.[4] Both Malvern and Rubin confine their attention to elastic unloading parallel to the initial slope of the static stress-strain curve.

The mathematical analysis is simplest when the characteristic directions are unchanged during the transition from loading to unloading. This suggests the use of infinitesimal strain theory and a linear unloading law such that unloading shock waves propagate with constant velocity equal to that of the initial wave front. Under these conditions the mechanical shock conditions are sufficient to determine the subsequent motion. In the general

case when the characteristic directions in front of and behind the shock are not parallel, we must assume some form for the dependence of internal energy on stress and strain which is utilized in forming the Hugoniot function. The Hugoniot function, in conjunction with the mechanical shock conditions, is sufficient to determine the jumps in stress and strain across the unloading shock. Since the stress-strain law that the material obeys once unloading commences differs from that during loading, it is plausible also to use a different internal energy function. However, we will show that this assumption prevents the shock wave from ever being completely absorbed. The situation for different internal energy functions across the shock is similar to that for detonation waves where an explosive mixture undergoes a change of state across the detonation front. Processes of this type are discussed by Courant and Friedrichs[5]; however, their analysis cannot be directly applied to the problem at hand unless we generalize the concept of the Hugoniot function along the lines suggested by Duvall.[6] This generalization takes into account the region of variable state into which the shock wave moves.

Because of the intractability of the mathematics in the general case, the physical processes are obscured. To obtain some insight into the problem, we review Malvern's description of the elastic unloading process from a more descriptive point of view before considering the general case.

Malvern's discussion of the unloading phenomena when the stress at $x = 0$ is instantaneously reduced to zero and maintained at that value follows. See Figure I. An unloading shock wave propagates along the C_+ characteristic from the point $x = 0$, $t = t_o$ at which the stress is released. This shock decreases in amplitude and may or may not be absorbed. The boundary between the elastic and viscoelastic states is identical with the shock path until the shock strength goes to zero, at which point the elastic-viscoelastic boundary leaves the C_+ characteristic and must be found by a trial-and-error method. Rubin, after linearizing the equations, uses asymptotic methods to show that an unloading shock is always absorbed in a finite time.

We present an alternative method for calculating the elastic-viscoelastic boundary after it leaves the C_+ characteristic and its subsequent interaction with elastic waves. While this alternative method appears to be more adaptable to programming for numerical calculation than Malvern's, the two methods are equivalent and should give identical answers. Malvern's description of the unloading phenomena is also modified to include the case that the material behind the unloading shock is in the viscoelastic state. This theory

is illustrated by tracing qualitatively the changes a rectangular stress pulse of amplitude σ_o and duration t_o applied at x = 0 undergoes as it propagates into the material.

THEORY

The dynamic behavior of the material can be illustrated by outlining those regions of the stress-strain plane that contain physically attainable values for these variables. In Figure II, $g(\sigma) = f(\varepsilon)$ is the static stress-strain law during loading. The line $\sigma = E\,\varepsilon$ is the continuation of the initial slope of the curve $g(\sigma) = f(\varepsilon)$. The line $\sigma = \frac{b}{a}\,\varepsilon$ is the locus of stress-strain pairs at infinite strain rate. Regions II and III are the locus of points for the viscoelastic state. Region I is the locus of points where the material has become elastic; any point in Region I must be connected to a point in Regions II or III by an unloading shock wave.

A material governed by Malvern's theory could only assume values in Region II of Figure II during the loading portion of a complete stress cycle. Hence, Malvern's theory predicts that Young's modulus E calculated from any dynamic test will never exceed E obtained during a static test. However, experimenters in soil mechanics report increases as high as 30% in Young's modulus when measured dynamically over the value obtained in static tests.[7] The present theory adds Region III to the set of attainable stress-strain pairs of Malvern's theory to allow this apparent increase in Young's modulus with increasing strain rate. This generalization of Malvern's theory is obtained by introducing an additional dynamic constant b to

supplement Malvern's dynamic constant k which is identical to 1/a in the present theory.

Qualitatively correct wave shapes can be deduced without resorting to numerical analysis for the special case of infinitesimal strain theory and linear unloading with slope b/a from any point in Region I. Under these assumptions, the characteristic directions for the complete stress cycle are the family of straight lines $x = \pm\sqrt{b/a\rho}\,t$ + constant. In contrast to plastic materials, stress and strain are not constant along these characteristics because nonlinear viscoelastic materials do not possess simple wave solutions. A physical explanation for the absence of a simple wave solution is discussed in a previous report.[8] However, much physical insight can still be gleaned by considering the variation of stress and strain along individual $C_+^{(n)}$ characteristics as a function of time. With reference to Figure III, σ and ε along $C_+^{(0)}$ are related by $\sigma = \frac{b}{a}\varepsilon$. This is the line segment A-A' in the stress-strain plane shown in Figure IV. The origin in Figure III where the stress rises discontinuously from zero to σ_o transforms to the point A in Figure IV. As this decaying shock propagates into the material, the associated values of σ and ε move down the line segment from A to A' as t increases from 0 to ∞.

The values to stress and strain associated with the point B, which is where $C_+^{(1)}$ intersects x= 0, differ from those associated with A because the strain has increased in the time interval from A to B. The actual path taken through the σ, ε plane along $C_+^{(1)}$ is not known but, because of continuity, it must be reasonably close to A-A', never intersecting A-A'. This path is shown schematically as B-B'. Thus the motion can be described qualitatively by plotting the variation of σ and ε along any $C_+^{(n)}$ characteristic through the σ, ε plane from σ_0 at x = 0 to some point on $g(\sigma) = f(\varepsilon)$ as t approaches ∞. These paths through the σ, ε plane are shown as A-A', B-B', C-C', D-D', ect., in Figure IV.

At t_0, where $C_+^{(n)}$ originates, the stress is instantaneously reduced to zero. Then the values of stress and strain at the back of the resulting shock are connected to the values in front of the shock, which are plotted at the point θ_1 by a line parellel to A-A', terminating at $\sigma = 0$; i.e., the point ϕ_2 in Figure IV. The values of stress and strain in front of and in back of the shock are connected by this path because unloading in the viscoelastic Regions II and III follows such paths for the infinite strain rate generated by the step in stress. By hypothesis, the material unloads in Region I along this path, independently of the strain rate.

At x = 0, we were able to calculate $\Delta\varepsilon$ across the shock because we knew $\Delta\sigma$ from the boundary condition. However when $x \neq 0$, we will have to calculate $\Delta\sigma$ from the characteristic equations and the mechanical jump conditions. Note that the foot of the shock is well within Region I, at least for small x. This situation is identical to Malvern's, and the equation for $\Delta\sigma$ in terms of the known quantities along $\theta_1 - \theta_1'$ is

$$\Delta\sigma\left(\frac{x}{c}, t-t_0\right) = \Delta\sigma(0,0) - \frac{1}{2a}\int_0^{t-t_0}\left[g(\sigma) - f(\varepsilon)\right]dt \qquad (1)$$

This equation is derived* by subtracting the characteristic equations valid along $C_+^{(n)}$ in front of and behind the shock and using the mechanical jump conditions.

Rubin showed that a linearized form of (1) always vanishes for some finite value of t, say point Q in Figures III and IV. Before (1) vanishes, $\Delta\sigma$ will reach a point P such that the values of stress and strain at the foot of the shock lie on $g(\sigma) = f(\varepsilon)$; i.e., the point ϕ_2' in Figure IV. Beyond this point we assume that the material is viscoelastic since the foot of the shock lies above the static curve. Because of this change, (1) is no longer applicable for computing $\Delta\sigma$. With the mechanical jump conditions and the altered characteristic equations

*See Appendix II.

in front of and behind the shock, (1) becomes*

$$\Delta\sigma\left(\frac{x}{c}, t - t_0\right) = \Delta\sigma(P) - \frac{1}{2a}\int_{t_P}^{t}\left\{\left(g(\sigma_1) - g(\sigma_2)\right) - \left(f(\varepsilon_1) - f(\varepsilon_2)\right)\right\} dt \quad (2)$$

where

σ_1, ε_1 = stress, strain along $P - Q - Q_1$

σ_2, ε_2 = stress, strain along $\phi_2' - Q_1$

t_p = time at point P

$\Delta\sigma(P)$ = $\Delta\sigma$ at P calculated from (1) at t = t_p

The stress-strain path at the foot of the shock is no longer $\phi_2 - \phi_2'$ to Q as shown, but follows some path $\phi_2 - \phi_2' - Q_1$ with a discontinuity in slope at ϕ_2'. This can be seen by rewriting (1) and (2) in differential form and sketching their graphs. Equations (1) and (2) can be written as

$$\frac{d\Delta\sigma}{dt} = \frac{-1}{2a}\left[g(\sigma_1) - f(\varepsilon_1)\right] \quad (3)$$

$$\frac{d\Delta\sigma}{dt} = \frac{-1}{2a}\left[\left(g(\sigma_1) - g(\sigma_2)\right) - \left(f(\varepsilon_1) - f(\varepsilon_2)\right)\right] \quad (4)$$

where subscripts 1 and 2 refer to points along the paths $\theta_1 - Q_1$

*See Appendix II.

and $\phi_2 - \phi_2' - Q_1$. In (3) the term $g(\sigma_1) - f(\varepsilon_1)$, at a typical point $t < t_p$, is represented graphically as the line segment R-R'. At time t_o, $g(\sigma_1) - f(\varepsilon_1)$ is represented graphically as the line segment $\theta_1 - \alpha_1$; from Figure IV, it is a monotonically decreasing function of time as R moves from θ_1 to P. If the material did not cross the elastic-viscoelastic boundary, R would continue along $\theta_1 - P$ to Q where the shock would be absorbed and then from Q to θ_1' where $g(\sigma_1) - f(\varepsilon_1)$ would go to zero at t = ∞ . Hence we can visualize (3) graphically as shown in Figure V.

From (1) we see that the area under this curve from x = 0 to t_Q is numerically equal to $\Delta\sigma(0,0)$. Equations (3) and (4) are equal at t , because at this point the second term on the right of (4) is zero. From Figure IV it is apparent that $g(\sigma) - f(\varepsilon) \geq 0$ for all t and that $g(\sigma_1) - f(\varepsilon_1) \geq g(\sigma_2) - f(\varepsilon_2) \geq 0$ for $t \geq t_p$ where the foot of the shock lies in Region II. Thus for $t > t_p$, $\frac{d^2\Delta\sigma}{dt^2}$ computed from (4) will be below the corresponding value computed from (3). We can also show that at $t = t_p$, $\frac{d^2\Delta\sigma}{dt^2}$ computed from (3) and (4) differs by an amount

$$\left.\frac{d^2\Delta\sigma}{dt^2}\right)_{(4)}_{t_p} - \left.\frac{d^2\Delta\sigma}{dt^2}\right)_{(3)}_{t_p} = \frac{-1}{2a}\left[\frac{d}{dt}\left\{g(\sigma_2) - f(\varepsilon_2)\right\}\right]_{t_p}$$

Therefore, in Figure V there will be a discontinuity in slope at t_ρ ; the new locus of points will plot below the curve computed from (3) for all $t > t_\rho$ as shown in Figure VI. The time at which the shock is absorbed must be increased to t_{Q1} , so that the area under the new curves in Figure VI from t_ρ to t_{Q_1} is equal to the area under the curve from t_ρ to t_Q in Figure V. We must now admit the possibility that the shock is never absorbed. From Figure IV , the stress-strain path at the foot of the shock now branches at ϕ_2' with a discontinuity in slope, and, if absorbed, it intersects the path in front of the shock at the point Q_1. The path segment $\phi_2' - Q_1$ is shown intersecting the path $\theta_1 - \theta_1'$ with different slope. Although this is not proved and must be verified by numerical calculations, it seems physically plausible that when the shock strength goes to zero, a discontinuity in the derivatives of stress and strain remains. This can be visualized by realizing that the peaks of the resulting wave forms are cusped. If this discontinuity did not exist, the wave peaks would be smooth.

As shown in Figure III, the x-t plane can be divided into four areas. Area E is the loading pulse and is characterized by increasing stress and strain as functions of time. These stress- strain points fall in Regions II and III of Figure II; the stress-strain paths are the lines A-A', B-B', etc., in

Figure IV. Area F is characterized by being entirely elastic with the stress, strain, and particle velocity known along the foot of the unloading shock which precedes it. Area G is also elastic but differs from Area F because the visco-elastic-elastic boundary preceding it is unknown and must be calculated by special techniques. Although Area H is viscoelastic, it differs from Area E because the stress and strain are decreasing functions of time.

The solution in Area F can be obtained by the principle of superposition. Assume that the necessary calculations have been made to obtain σ, ε, and v at the foot of the unloading shock. Let S be a parameter measuring distance along the unloading shock. Along this path σ, ε, and v are given by

$$\sigma(S) = \sigma_1 - \Delta\sigma$$

$$\varepsilon(S) = \varepsilon_1 - \frac{\Delta\sigma}{\rho c^2}$$

$$v(S) = v_1 + \frac{\Delta\sigma}{\rho c}$$

Along the boundary x = 0 the stress is $\sigma(0,t) = 0$ for $t \geq t_0$.

By the principle of superposition, the stress at any point (x,t) in Area F is

$$\sigma(x,t) = \sigma\left(x, t_0 + \frac{x}{c}\right) + \int_{x}^{\frac{1}{2}(x+c(t+t_0))} \sigma'(s)\,ds - \int_{0}^{\frac{1}{2}(c(t+t_0)-x)} \sigma'(s)\,ds \qquad (5)$$

The stress-strain relation in Area F is

$$\sigma(s) - \sigma = \frac{E}{\alpha}\left(\varepsilon(s) - \varepsilon\right) \qquad (6)$$

With (5), (6) becomes

$$\varepsilon(x,t) = \varepsilon\left(x, t_0 + \frac{x}{c}\right) + \frac{E}{\alpha}\int_{x}^{\frac{1}{2}(x+c(t+t_0))} \sigma'(s)\,ds - \frac{E}{\alpha}\int_{0}^{\frac{1}{2}(c(t+t_0)-x)} \sigma'(s)\,ds \qquad (7)$$

Note that $\varepsilon(0,t) = \varepsilon(0,t_0)$ in Area F.

We now wish to trace the elastic-viscoelastic boundary after it leaves the $C_+^{(n)}$ characteristic. Moving along the characteristic $C_+^{(n+1)}$ from x = 0, we first traverse the elastic Area F where the solution is known. This is the path segment $\phi_2 - \phi_2''$ in Figure IV where ϕ_2'' represents the boundary between Areas F and G.

The calculation of the elastic-viscoelastic boundary will be illustrated in Figure VII which is an enlargement of Figure III in the neighborhood of P. We

know that $g(\sigma) = f(\varepsilon)$ along the elastic-viscoelastic boundary after it leaves the $C_+^{(n)}$ characteristic. At point P_1 where this boundary cuts $C_+^{(n+1)}$, the following characteristic equations hold:

a. Along C_-

$$(\sigma_{P_1} - \sigma_{C_2}) + \rho C (V_{P_1} - V_{C_2}) = \frac{-1}{2a} \left[g(\sigma_{C_2}) - f(\varepsilon_{C_2}) \right] \Delta t \quad (8)$$

b. Along C_o

$$(\sigma_{P_1} - \sigma_{C_1}) - \rho C^2 (\varepsilon_{P_1} - \varepsilon_{C_1}) = \frac{-1}{2a} \left[g(\sigma_{C_1}) - f(\varepsilon_{C_1}) \right] \Delta t \quad (9)$$

At P_1, σ, ε, and V are related by the characteristic equations for a non-linear elastic material governed by $g(\sigma) = f(\varepsilon)$

$$V_{P_1} = -\int_0^{\varepsilon_{P_1}} C(\varepsilon)\, d\varepsilon = -\frac{1}{\rho} \int_0^{\sigma_{P_1}} \frac{d\sigma}{C(\sigma)} \quad (10)$$

where $C(\varepsilon)$ and $C(\sigma)$ are derivable from $g(\sigma) = f(\varepsilon)$. With (10), (8) and (9) can be written

$$(\sigma_{P_1} - \sigma_{C_2}) + \rho C \left[-\frac{1}{\rho} \int_0^{\sigma_{P_1}} \frac{d\sigma}{C(\sigma)} - V_{C_2} \right] = -\frac{\Delta t}{2a} \left[g(\sigma_{C_2}) - f(\varepsilon_{C_2}) \right] \quad (11)$$

$$(\sigma_{P_1} - \sigma_{C_1}) - \rho C^2\left[\frac{1}{\rho}\int_0^{\sigma_{P_1}} \frac{d\sigma}{C^2(\sigma)} - \varepsilon_{C_1}\right] = \frac{-\Delta\tau}{2a}\left[g(\tau_1) - f(\varepsilon_{C_1})\right] \quad (12)$$

which gives σ_{P_1} implicitly as function of known quantities along $C_+^{(n)}$. The calculation procedure follows: assume $x_{P_1} = x_P$, solve (11) and (12) for σ_{P_1}, and compare them. If the values of σ_{P_1} calculated from (11) and (12) are unequal, move x_{P_1} along $C_+^{(n+1)}$ an increment δS and repeat the calculation. Repeat this procedure until the σ_{P_1}'s from (11) and (12) are equal. This is the correct location of the boundary.

This procedure for calculating the elastic-viscoelastic boundary assumes no interaction with other waves. However, as soon as the viscoelastic boundary leaves the C_+ characteristic, elastic unloading waves overtake it and modify both its position and associated values of stress, strain, and particle velocity.

To simplify the analysis, consider the unloading wave as made up of n stress increments of magnitude $\Delta\sigma$ separated by time intervals $\Delta\tau$. The first unloading increment propagates along $C_+^{(n+1)}$

through the elastic Region F. There is no interaction in this region except a change in the level of the stress increment as it encounters the rising stress level radiated from the back of the unloading shock. This unloading increment meets the elastic-viscoelastic boundary at the point P_1 in Figure VII. Since the strain-rate associated with this step is infinite, changes in stress and strain are given by the shock conditions. Hence at P_1 we know both $\Delta\sigma$ and $\Delta\varepsilon$. This situation is now identical to the previous analysis along $C_+^{(n)}$ at the origin. The increment $\Delta\sigma$ will move into the viscoelastic area along $C_+^{(n+1)}$. Initially, the foot of this small shock will be below the elastic-viscoelastic boundary. The decrease in magnitude of the increment $\Delta\sigma$, as it penetrates the viscoelastic area, is governed by (1) until a new point P along $C_+^{(n+1)}$ is reached, such that the foot of this shock lies on $g(\sigma) = f(\varepsilon)$. At this point the elastic-viscoelastic boundary again leaves the C_+ characteristic; the law controlling the decay in shock strength changes from (1) to (2). Further along $C_+^{(n+1)}$, the increment may eventually be absorbed at a point Q_1. The n unloading stress increments impinge upon the elastic-viscoelastic boundary in succession along the C_+ characteristic as shown in Figure VIII. The

procedure can be extended indefinitely by generalizing the parameter S and hence the functions $\sigma(s)$, etc., in (5) and (7), so that they follow the elastic-viscoelastic boundary after it leaves the $C_+^{(n)}$ characteristic at P. For this extension the limits of integration must be modified. This procedure extends the region in which (5) and (7) are valid to include G in Figure III.

The curvature of the boundary after it leaves $C_+^{(n)}$ can also be deduced from this analysis. As shown in Figures III, VII, and VIII, the velocity associated with the boundary decreases with time and distance. This immediately raises the question whether the boundary even comes to rest, so that some portion of the material remains viscoelastic and hence deforms forever. This will be shown not to be the case. The velocity of the boundary approaches a limit controlled by the static parameters of the material. Recall that along this boundary $g(\sigma) = f(\varepsilon)$ and that changes in stress, strain, and particle velocity are interrelated by equations (10) which are derived from the characteristic equations of a plastic material. Hence along this boundary - and only this boundary - the material behaves plastically with the stress-strain curve $g(\sigma) = f(\varepsilon)$.

These characteristic equations are known to be valid only along the characteristic directions associated with the stress and strain at a given point. Since σ and ε vary along this boundary, the characteristic direction continuously varies; hence the boundary must be an envelope of characteristic directions of the plastic material defined by the static stress-strain curve. Since the stress and strain decrease along this boundary, the associated velocity will increase or decrease as the static curve is concave or convex to the strain axis. The limiting velocity which the elastic-viscoelastic boundary approaches is determined by the initial slope of $g(\sigma) = f(\varepsilon)$; i.e., $C = \sqrt{\frac{E}{\rho}} \neq 0$, which must be less than or equal to $C = \sqrt{\frac{\nu}{a\rho}}$. Regardless of whether the velocity increases or decreases, the material becomes entirely elastic. However if $\sqrt{\frac{E}{\rho}} < \sqrt{\frac{\nu}{a\rho}}$, the viscoelastic region increases in width; while if they are equal, the width approaches a limiting value.

Examination of (5) and (7) shows that as $t \rightarrow \infty$, the stress distribution goes to zero leaving a non-zero strain distribution calculated from

$$\varepsilon(x,\infty) = \varepsilon(s) - \frac{a}{\nu}\sigma(s) \qquad (13)$$

We are now able to describe qualitatively the resulting wave shapes, having considered how σ and ε vary along the C_+ family of characteristics and noting the changes required by conservation of mass and momentum as the boundaries between various regions in the x-t plane are crossed.

First, consider the time variation of σ and ε at x = 0. The former is known since it is the boundary condition. The latter is known to be an immediate elastic response, ε_0, followed by flow asymptotically tending to the value ε_∞. The quantity ε_∞ is given by the solution of $g(\sigma_0) = f(\varepsilon_\infty)$ and is shown in Figure II. Hence ε_∞ is the maximum strain the material would attain if there were no time-rate effects, with the same boundary condition. At t_0, the stress is instantaneously reduced to zero. This is illustrated by the path $\theta_1 - \phi_2$ in Figure IV. A sketch of these wave shapes is shown in Figure IX.

Consider the time variation of σ and ε at a point intermediate between x = 0 and x_ρ in Figure III. The stress remains zero until a time t = x/c when the initially discontinuous wave fronts of amplitude $\sigma(\frac{x}{c})$, $\varepsilon(\frac{x}{c})$ arrive. These wave fronts are followed by a

period of increasing stress and strain tending asymptotically to the values σ_0 , ε_∞ until a time $t_0 + x/c$ when the unloading shock wave arrives, instantaneously reducing the stress and strain. The variation of stress and strain behind the unloading shock is given by (5) and (7), showing that the stress asymptotically approaches zero and the strain approaches the value $\varepsilon(x, \infty)$ given by (13), as shown schematically in Figure X.

The first transition point occurs at x_p where the elastic-viscoelastic boundary first leaves the $C_+^{(n)}$ characteristic. The wave shape will be similar in form to those shown in Figure X. However the magnitudes of the initial elastic loading shock, the subsequent unloading shock, and the residual strain $\varepsilon(x, \infty)$ will all decrease. These changes are shown schematically in Figure XI.

In the interval x_p to x_{Q_1} in Figure III, the wave form will differ from those depicted in Figure X and XI due to the development of Area H. In this area, characterized by paths below $\phi_2' - Q_1$ in Figure IV, the material is viscoelastic with σ and ε decreasing. This viscoelastic unloading portion of the pulse is bounded by the elastic-viscoelastic boundary.

The stress and strain variation at a point x between x_P and x_{Q_1} is sketched in Figure XII.

The second transition point is x_{Q_1} where the unloading shock is absorbed. As discussed earlier, there remains a discontinuity in the derivatives of σ and ε, so that the wave crest is cusped as shown in Figure XIII.

It is known from the mathematical theory of characteristics that discontinuities in the derivatives of σ and ε propagate along the characteristic directions. Hence for infinitesimal strain theory, the duration of the loading portion shown as Area E in Figure IV remains constant and of duration t_o, in contrast with experimentally observed pulse shapes in metals and earth materials. One way to modify the theory so that the loading zone increases in duration, is to require the equations for the characteristic directions to contain the dependent variables. A physically plausible method of accomplishing this is to include the second order terms in the strain-displacement law, thus making the transition to finite-strain theory.

As discussed in the previous report[8], the transition to finite strain theory requires that an unloading shock wave propagate along the C_+ characteristic emanating from the point $x = 0$, $t = t_o$, with variable velocity

depending on the strain in the region into which it is moving. To analyze the variation of shock intensity when the characteristic directions are variable and, in general, not parallel to the characteristic directions at the foot of the shock, we assume:

1. The stress-strain law during the loading cycle

$$a\sigma_t - b\alpha_t = f(\alpha) - g(\sigma)$$

2. The stress-strain law during the unloading cycle

$$\sigma(s) - \sigma = F(\alpha(s) - \alpha)$$

subject to the condition (14)

$$\sqrt{\frac{F'(\alpha(s)-\alpha)}{\rho}} \leq c(\varepsilon_\infty)$$

3. The internal energy during the loading cycle

$$E_\ell = \lambda_1 \sigma^2 + \lambda_2 \sigma\alpha + \lambda_3 \alpha^2 \tag{15}$$

4. The internal energy during the unloading cycle

$$E_u = \beta_1 \sigma^2 + \beta_2 \sigma\alpha + \beta_3 \alpha^2 \tag{16}$$

5. The first law of thermodynamics

$$dE = -\sigma d\alpha + dQ \tag{17}$$

With these definitions and assumptions, the well-known Hugoniot function becomes

$$E_u(\sigma_2, \alpha_2) - E_\ell(\sigma_1, \alpha_1) = \frac{-1}{2}(\alpha_2 - \alpha_1)(\sigma_2 + \sigma_1) \quad (18)$$

Subcripts 1 and 2 refer, respectively, to points at the top and bottom of the shock. Write the variables at the foot of the shock in terms of the jumps in stress and strain and their values in front of the shock:

$$\begin{aligned} \sigma_2 &= \sigma_1 - \Delta\sigma \\ \alpha_2 &= \alpha_1 - \Delta\alpha \\ V_2 &= V_1 - \Delta V \end{aligned} \quad (19)$$

Then (18) becomes

$$E_u(\sigma_1 - \Delta\sigma, \alpha_1 - \Delta\alpha) - E_\ell(\sigma_1, \alpha_1) = \frac{-\Delta\alpha}{2}(2\sigma_1 - \Delta\sigma) \quad (20)$$

Write $\Delta\alpha$ in terms of $\Delta\sigma$ using the mechanical shock conditions remembering that the shock velocity is a function of ε_1 :

$$\Delta\alpha = \frac{\Delta\sigma}{\rho C^2(\varepsilon_1)} \quad (21)$$

Hence (20) can be written as an implicit function of $\Delta\sigma$ and known quantities at the top of the shock:

$$E_u\left(\sigma_1-\Delta\sigma,\alpha_1-\frac{\Delta\sigma}{\rho c^2(\varepsilon_1)}\right)-E_\ell(\sigma_1,\alpha_1)=-\frac{\Delta\sigma}{\rho c^2(\varepsilon_1)}\left(2\sigma_1-\Delta\sigma\right) \qquad (22)$$

It is interesting to note the restrictions placed on the internal energy functions if experimental evidence shows the unloading shock is absorbed. If we place $\Delta\sigma=0$, (22) reduces to

$$E_u(\sigma_1,\alpha_1) = E_\ell(\sigma_1,\alpha_1) \qquad (23)$$

where σ_1 and α_1 are not constants. This requires that E_u and E_ℓ be identical in form over some range of σ and α that must be determined experimentally. Over this range, one function will represent the internal energy independently of the equation of state during different portions of a complete stress cycle.

We illustrate the numerical calculations necessary to determine the jumps in stress, strain, and particle velocity,using (15) and (16) to define the

internal energy. Thus (22) becomes

$$A_1 \Delta\sigma^2 + A_2 \Delta\sigma + A_3 = 0 \tag{24}$$

where

$$A_1 = \beta_1 + \frac{\beta_2}{\rho C^2(\varepsilon_1)} + \frac{\beta_3}{\rho^2 C^4(\varepsilon_1)} - \frac{1}{2\rho C^2(\varepsilon_1)}$$

$$A_2 = \frac{\sigma_1}{\rho C^2(\varepsilon_1)} - 2\beta_1\sigma_1 - \beta_2\left(\alpha_1 - \frac{\sigma_1}{\rho C^2(\varepsilon_1)}\right) - \frac{2\beta_3\alpha_1}{\rho C^2(\varepsilon_1)} \tag{25}$$

$$A_3 = (\beta_1 - \lambda_1)\sigma_1^2 + (\beta_2 - \lambda_2)\sigma_1\alpha_1 + (\beta_3 - \lambda_3)\alpha_1^2$$

The quantities A_1, A_2, A_3 are evaluated in terms of the known stress and strain in front of the shock. Since (24) has two roots, that root must be chosen which is physically compatible with (19), the other being extraneous.

Application of (24) along the shock path determines the variation of stress, strain, and particle velocity along a path in the x-t plane. The unloading problem is completed by solving (14) simultaneously with the laws for conservation of mass and momentum, subject to the boundary condition $\sigma = 0$ at $x = 0$ and satisfying the previously obtained values of stress, strain, and

particle velocity at the foot of the shock wave. This analysis applies only when the shock path is not a characteristic in the unloading region. The problem is now reduced to a new and simpler boundary value problem with known methods of solution. Numerical solutions can be obtained using procedures described by Lister[9] for one-dimensional compressible fluid flow. These procedures are outlined in Appendix I.

SUMMARY

Qualitatively correct changes in shape of a rectangular stress pulse applied at the surface of a nonlinear viscoelastic material are obtained for the special case of infinitesimal strain theory and a linear unloading law, such that the characteristic directions during the entire stress cycle are unchanged. It is found that the limitation of infinitesimal strain does not permit pulse broadening during the loading portion of the stress cycle, which is at variance with experimentally observed stress waves in soils. The transition to finite strain, allowing for pulse broadening, complicates the unloading theory so that the mechanical shock conditions are not sufficient to determine the changes in stress, strain, and particle velocity across an unloading shock. By specifying the dependence of the internal energy on stress and strain for the material, it is possible to construct the Hugoniot function which, coupled with the mechanical shock conditions, is sufficient to determine the transition across the unloading shock.

Once the Hugoniot function for the material is

defined, it is possible to analyse the unloading shock for quite general unloading laws. Finally, the numerical procedures for completion of the analysis are outlined in a form suitable for programming for digital computers.

APPENDIX I

We outline the computational procedures for calculating the variation of stress, strain, and particle velocity behind the unloading shock wave for the finite strain case. The necessary modifications to reduce to infinitesimal strain theory are discussed at the end.

The equations to be solved are:

$$\sigma_\tau - F'(\alpha(s)-\alpha)\,\alpha_\tau = \sigma_\tau(s) - F'(\alpha(s)-\alpha)\,\alpha_\tau(s) \tag{26}$$

$$\sigma_x - \rho V_t = 0 \tag{27}$$

$$\alpha_\tau - V_x - \varepsilon \varepsilon_\tau = 0 \tag{28}$$

$$V_x - \varepsilon_\tau = 0 \tag{29}$$

Using, the techniques presented in the previous report[8], the set of characteristic equations and directions corresponding to (26)-(29) are found to be:

$$C_+: \quad \frac{dx}{dt} = \sqrt{\frac{F'(\alpha(s)-\alpha)(1+\varepsilon)}{\rho}} \tag{30}$$

$$d\sigma - \rho\sqrt{\frac{F'(\alpha(s)-\alpha)(1+\varepsilon)}{\rho}}\, dv = = \sigma_t(s) - F'(\alpha(s)-\alpha)\,\alpha_t(s) \tag{31}$$

$$C_-: \quad \frac{dx}{dt} = -\sqrt{\frac{F'(\alpha(s)-\alpha)(1+\varepsilon)}{\rho}} \tag{32}$$

$$d\sigma + \rho\sqrt{\frac{F'(\alpha(s)-\alpha)(1+\varepsilon)}{\rho}}\, dv = = \sigma_t(s) - F'(\alpha(s)-\alpha)\,\alpha_t(s) \tag{33}$$

$$C_0: \quad \frac{dx}{dt} = 0 \tag{34}$$

$$\sigma(s) - \sigma = F(\alpha(s) - \alpha) \qquad (14)$$

Where S is a parameter specifying position along the shock path.

The boundary conditions to be satisfied are:

(a) Along x = 0, $\sigma = 0$

$$\alpha = \alpha(s)_{s=0}$$

(b) Along the unloading side of the shock path $\sigma, \alpha, \varepsilon, V$ take on the values $\sigma(s), \alpha(s), \varepsilon(s), V(s)$ which have been previously calculated by the continuous solution of (24).

We are specifying the values for all the dependent variables along this path. For a solution to exist under these conditions, we require that the slope of the unloading shock path in the x-t plane measured by $\frac{dt}{dx}$ be everywhere less in absolute value than the slope of any characteristic for the unloading system which crosses it. The inequality associated with (14) is sufficient to satisfy this requirement. Under these restrictions, the set of characteristics in the unloading zone is shown schematically in Figure XIV.

Equations (14) and (30)-(34) as written are not in a suitable form for numerical calculation. We rewrite them

in incremental form after introducing the following notation where the relative position of points P, Q, R, S are illustrated in Figure XVI.

$$G(P) = \sqrt{\frac{F'(\alpha_{(S)}-\alpha)(1+\varepsilon)}{\rho}} \quad \text{evaluated at any point P.}$$

$$H(Q) = \sigma_t(S) - F'(\alpha_{(S)}-\alpha)\,\alpha_\tau(S) \quad \text{evaluated at any point Q.}$$

$$C\binom{P}{Q} = 1/2\,[G(P) + G(Q)]$$

$$D\binom{P}{Q} = 1/2\,[H(P) + H(Q)]$$

The last two expressions are approximations of the average value of G and H, respectively, along any line segment PQ. With this notation, the stress, strain, and particle velocity at a point P can be found in terms of the known stress, strain, and particle velocity at points Q, R, S by the simultaneous solution of :

along C_+

$$\sigma(P) - \rho C\binom{P}{S} V(P) = \sigma_{(S)} + D\binom{P}{S}\Delta\tau'' - \rho C\binom{P}{S} V(S) \qquad (35)$$

along C_-

$$\sigma(P) + \rho C\binom{P}{Q} V(P) = \sigma(Q) + D\binom{P}{Q}\Delta\tau' + \rho C\binom{P}{Q} V(Q) \qquad (36)$$

along C_o

$$\sigma(P) = \sigma(R) - F(\alpha(R) - \alpha(P)) \tag{37}$$

where $t_{(P)} - t_{(Q)} = \Delta t'$, $t_{(P)} - t_{(S)} = \Delta t''$.

The location of P and R are known by prechoosing the grid made up of increments ΔX and Δt . The location of Q and S must be found as part of the solution.

The calculation begins at a point P at time $t_o + \Delta t$ on x=0. At P, $\sigma, \alpha, \varepsilon$ are known. The point Q is the intersection of the C_- characteristic through P with the shock path. Once the point of intersection is established, all four variables are known there from previous calculations.

Since the equations are nonlinear, an iterative procedure is used to converge on the correct solution. In the following equations a bracketed superscript refers to the order of the iteration. Nonsuperscripted variables do not change during the iteration procedure at a given point. An iterative scheme for locating Q in Figure XV is:

$$t^{(n)}_{(Q)} = t_{(P)} - \frac{\Delta x}{C^{(n-1)}_{(P)(Q)}} \tag{38}$$

where $C^{(0)}\left(\frac{P}{Q}\right) = G(R)$

For n = 1 an initial estimate of $t^{(1)}(Q)$ yields a value G(Q) from which $t^{(2)}(Q)$ can be calculated. The iteration is continued until $\left|t^{(n)}(Q) - t^{(n-1)}(Q)\right| < \epsilon$ where ϵ is a prechosen accuracy factor.

Once t(Q) has been evaluated to the desired accuracy, the coefficients in (36) can be immediately evaluated and the equation solves for V(P).

The calculation at a point P not on the boundary is more complex. We illustrate this more general case in Figure XVI where the new P has been moved one ΔX unit to the right and remains one ΔT unit above the shock path. The points Q, R, S are respectively the intersection of the shock path with C_- and C_o through P, and the intersection of the previous C_o characteristic with C_+ through P. An equation from which the time $t^{(n)}(S)$ can be evaluated is

$$t^{(n)}_{(S)} = t_{(P)} - \frac{\Delta X}{C^{(n-1)}\left(\frac{P}{S}\right)} \qquad (39)$$

where $C^{(0)}\left(\frac{P}{S}\right) = G(R)$

To locate the point Q we assume the path of the unloading shock is expressible as some numerical function

$$t = \phi(x) \quad \text{or} \quad x = \phi^{-1}(t)$$

The point Q is found by solving the implicit function

$$\frac{X_{(P)} - X^{(n)}_{(Q)}}{t_{(P)} - \phi(X^{(n)}_{(Q)})} = C^{(n-1)}\begin{pmatrix} P \\ Q \end{pmatrix} \tag{40}$$

where

$$C^{(0)}\begin{pmatrix} P \\ Q \end{pmatrix} = G(R)$$

The coefficients in (35) and (36) can be evaluated by assuming the initial estimates

$$\sigma_P^{(0)} = \tfrac{1}{3}\left[\sigma^{(0)}(Q) + \sigma(R) + \sigma^{(0)}(S)\right]$$

$$\alpha^{(0)}(P) = \tfrac{1}{3}\left[\alpha^{(0)}(Q) + \alpha(R) + \alpha^{(0)}(S)\right]$$

$$V^{(0)}(P) = \tfrac{1}{3}\left[V^{(0)}(Q) + V(R) + V^{(0)}(S)\right]$$

$$G^{(0)}(P) = \tfrac{1}{3}\left[G^{(0)}(Q) + G(R) + G^{(0)}(S)\right]$$

$$H^{(0)}(P) = \tfrac{1}{3}\left[H^{(0)}(Q) + H(R) + H^{(0)}(S)\right]$$

These initial estimates are then used to calculate $\sigma^{(1)}(P)$, $V^{(1)}(P)$ by simultaneous solution of (35) and (36) and then solving (37) for $\alpha^{(1)}(P)$, since $\sigma^{(1)}(P)$ is known. These estimates are then used to evaluate more accurately the coefficients in (35) and (36); the problem is then resolved as described above. Processes of this nature are stable and solutions can be obtained to any desired degree of accuracy.

When the desired accuracy has been achieved, the calculation moves to a new P point one ΔX unit to the right and remaining one $\Delta \tau$ unit above the unloading shock path. The problem of evaluating the stress, strain, and particle velocity at this new point is identical to the previously described problem and the entire process is repeated. In this manner, the numerical solution is obtained along a line parallel to the original unloading shock path as far out as desired. This new path is then used as the base onto which another strip of solution can be added.

The above procedure was outlined for the more general finite strain theory. For many purposes, infinitesimal theory will suffice. The above process is readily modified to include the infinitesimal strain case by formally setting ε and its derivatives identically zero wherever they appear and considering α as the infinitesimal strain. Under this reduction, (29) becomes meaningless and should be ignored.

APPENDIX II

Malvern's derivations of (1) and (2) are straightforward. We repeat them here since his derivations are unpublished.

A characteristic equation valid along C_+ at the top of the shock is

$$d\sigma_1 - \rho C\, dV_1 = \frac{-1}{a}\left[g(\sigma_1) - f(\varepsilon_1)\right] dt \quad (41)$$

If the material at the foot of the shock is elastic with Young's modulus b/a, the characteristic equation corresponding to (1) is

$$\sigma_2 - \rho C V_2 = K \qquad = \text{constant} \quad (42)$$

The mechanical shock conditions yield

$$\sigma_1 - \sigma_2 = -\rho C (V_1 - V_2) \quad (43)$$

From (42) and (43),

$$\Delta\sigma = \frac{\sigma_1 - \rho C V_1}{2} + \frac{k}{2} \quad (44)$$

Taking the differential of (44) along C_+, one obtains

$$d\Delta\sigma = \frac{1}{2}\left(d\sigma_1 - \rho C\, dV_1\right) \quad (45)$$

Substitution of (41) in (45) gives

$$d\Delta\sigma = \frac{-1}{2a}\left(g(\sigma_1) - f(\varepsilon_1)\right) dt$$

Equation (1) is then obtained by integrating along C_+ from t_o at x = 0 to t.

To obtain (2), the characteristic equation at the foot of the shock is changed from (42) to

$$d\sigma_2 - \rho C\, dV_2 = \frac{-1}{a}\left(g(\sigma_2) - f(\varepsilon_2)\right) dt \qquad (46)$$

Now subtract (46) from (41) to obtain

$$d\sigma_1 - d\sigma_2 - \rho C(dV_1 - dV_2) = \\ = -\frac{1}{a}\left[(g(\sigma_1) - g(\sigma_2)) - (f(\varepsilon_1) - f(\varepsilon_2))\right] dt \qquad (47)$$

Rewrite (43) in differential form

$$d\sigma_1 - d\sigma_2 = \rho C\, dV_2 - \rho C\, dV_1 \qquad (48)$$

Solve (48) for dV_2 and substitute into (47) to obtain:

$$d\sigma_1 - d\sigma_2 - \rho C\, dV_1 + d\sigma_1 - d\sigma_2 + \rho C\, dV_1 = \\ = \frac{-1}{a}\left[(g(\sigma_1) - g(\sigma_2)) - (f(\varepsilon_1) - f(\varepsilon_2))\right] dt \qquad (50)$$

Collecting terms and using $d\sigma_1 - d\sigma_2 = d(\Delta\sigma)$ one obtains

$$d\Delta\sigma = \frac{-1}{2a}\left[(g(\sigma_1) - g(\sigma_2)) - (f(\varepsilon_1) - f(\varepsilon_2))\right] dt \,,$$

from which (2) may be obtained by integration along C_+ from t_o to t.

REFERENCES

1. Lee, E. H., "A Boundary Value Problem in the Theory of Plastic Wave Propagation", Quart. Appl. Math. 10, 335, 1953.

2. Morland, L. W., "The Propagation of Plane Irrotational Waves Through an Elastoplastic Medium", Phil. Trans. Roy. Soc. Lond. A, 251, 341-383, 1959.

3. Malvern, L. E., "The Propagation of Longitudinal Waves of Plastic Deformation in a Bar of Material Exhibiting a Strain-Rate Effect", Ph.D. Thesis, Brown University, 1949.

4. Rubin, R. J., "Propagation of Longitudinal Deformation Waves in a Prestressed Rod of Material Exhibiting a Strain-Rate Effect", J. Appl. Phys. 25, 1954.

5. Courant, R., and Friedrichs, K.O., Supersonic Flow and Shock Waves, INTERSCIENCE, 1948.

6. Duvall, G. E., "Shock Wave Stability in Solids", Poulter Laboratories, Stanford Research Institude, Menlo Park, California.

7. Whitman, R. V., et al., "The Behavior of Soils Under Dynamic Loadings", Final Report on Laboratory Studies, MIT, Department of Civil and Sanitary Engineering Soil Mechanics Laboratory, August 1954, AFSWP-118, Contract DA-49-129 Eng-227, Office of the Chief of Engineers.

8. Mercado, E. J., "Stress Propagation in Nonlinear Viscoelastic Materials", Tech. Rept. No. 3, Ballistic Research Laboratories, Contract No. DA-115-509-ORD-1009, May 1, 1962.

9. Lister, Mary, The Numerical Solution of Hyperbolic Partial Differential Equations by the Method of Characteristics, Mathematical Methods for Digital Computers, John Wiley, 1961.

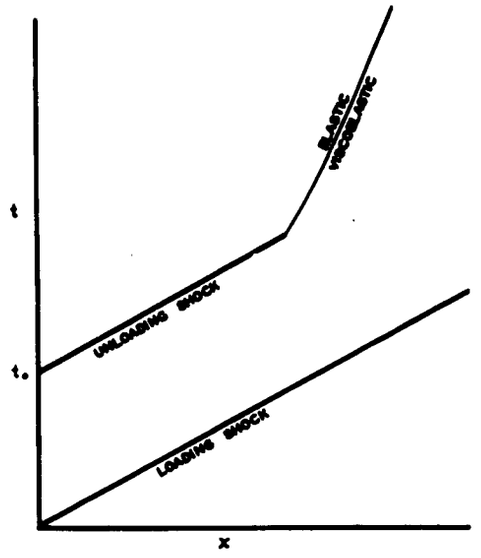

FIGURE I

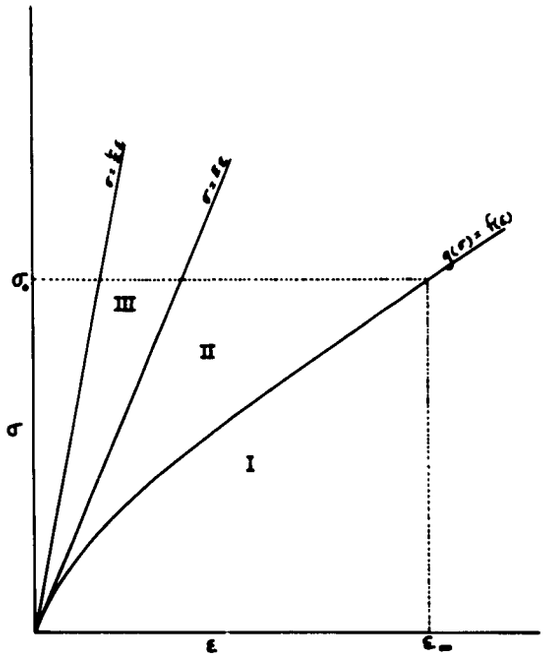

FIGURE II

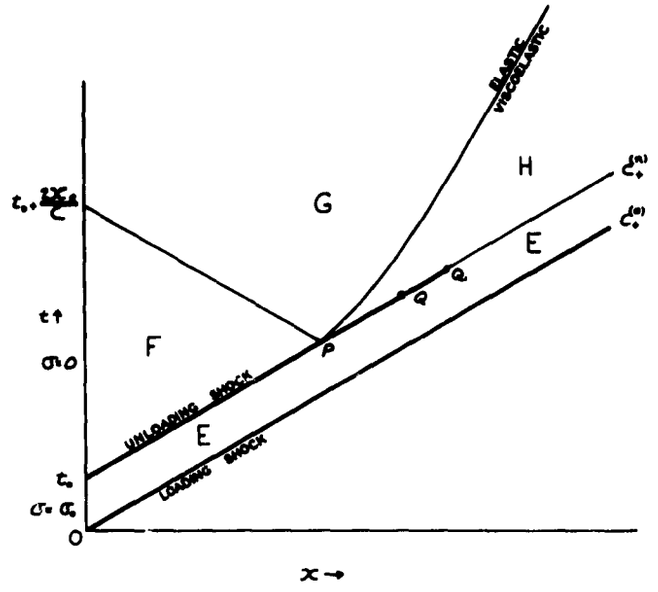

FIGURE III

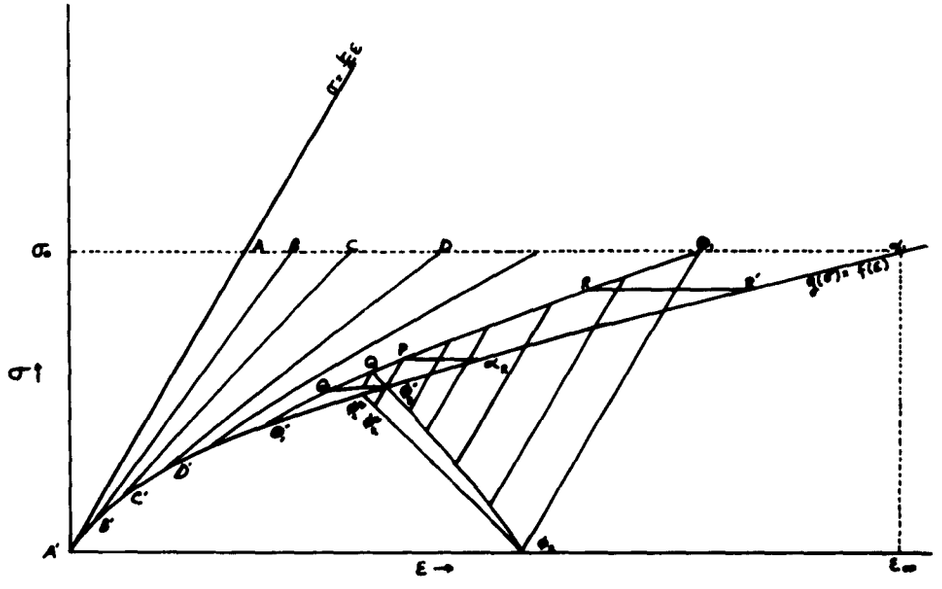

FIGURE IV

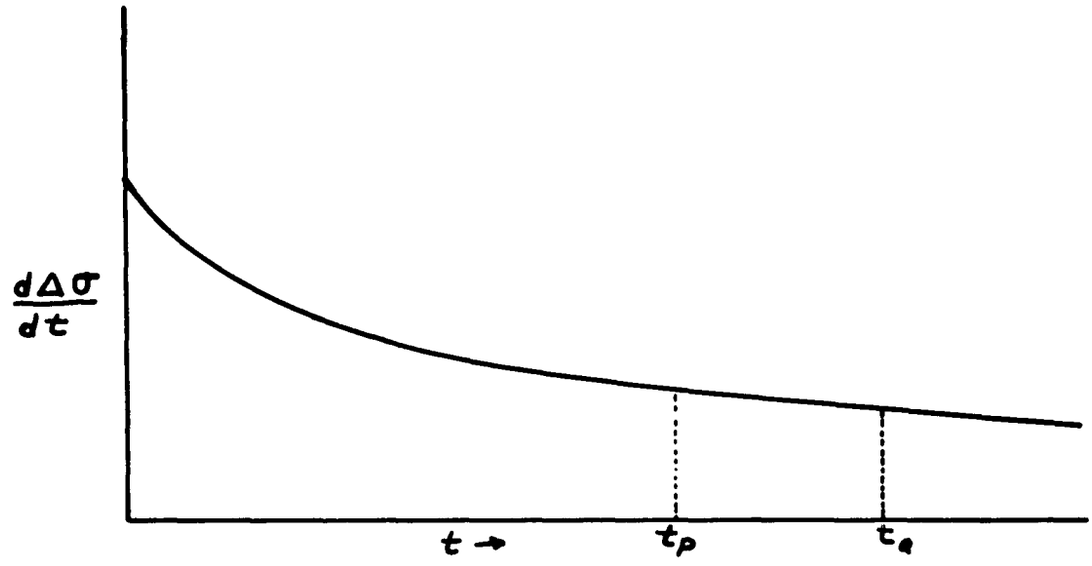

FIGURE V

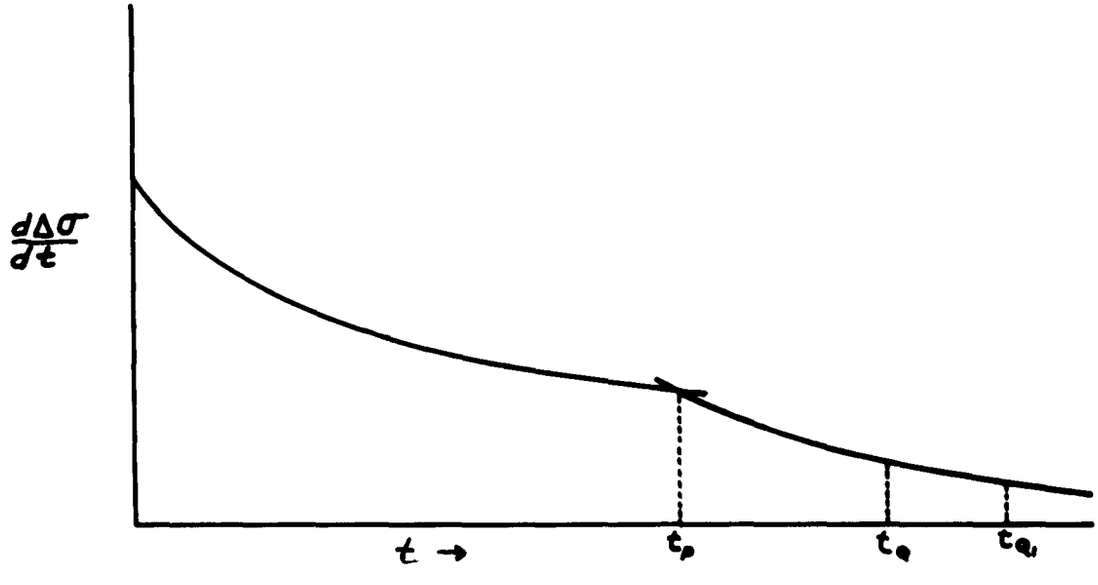

FIGURE VI

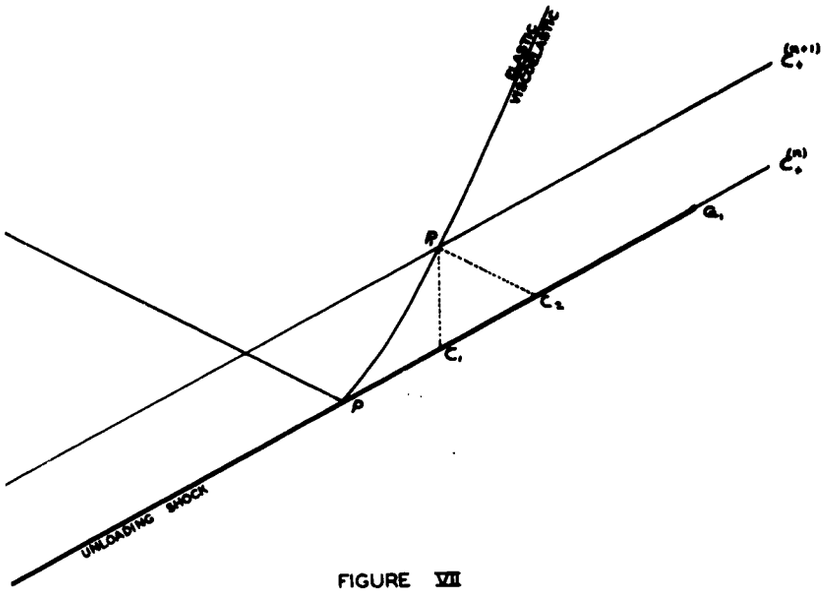

FIGURE VII

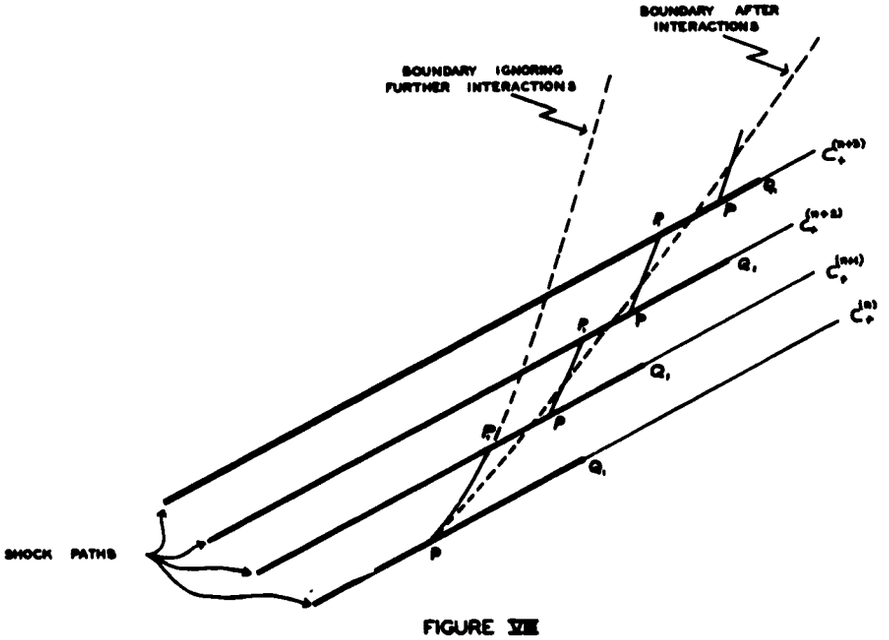

FIGURE VIII

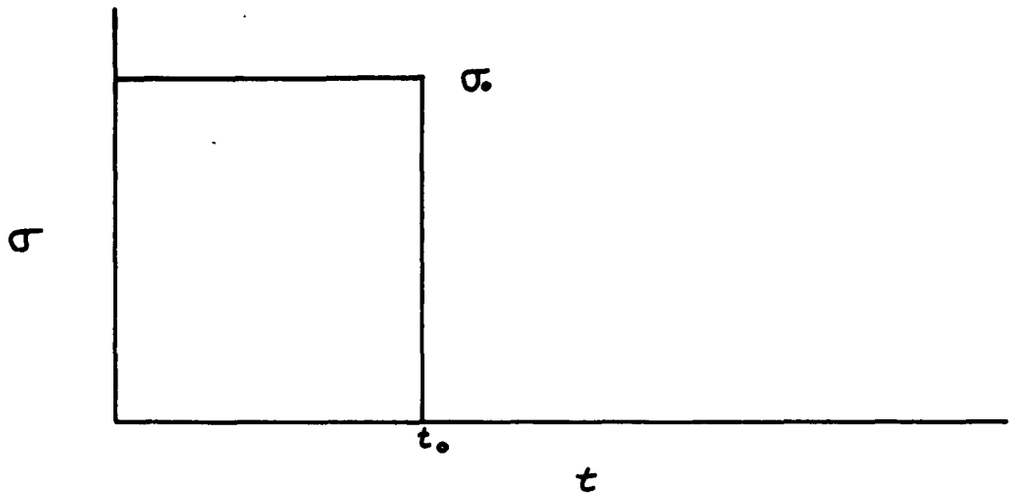

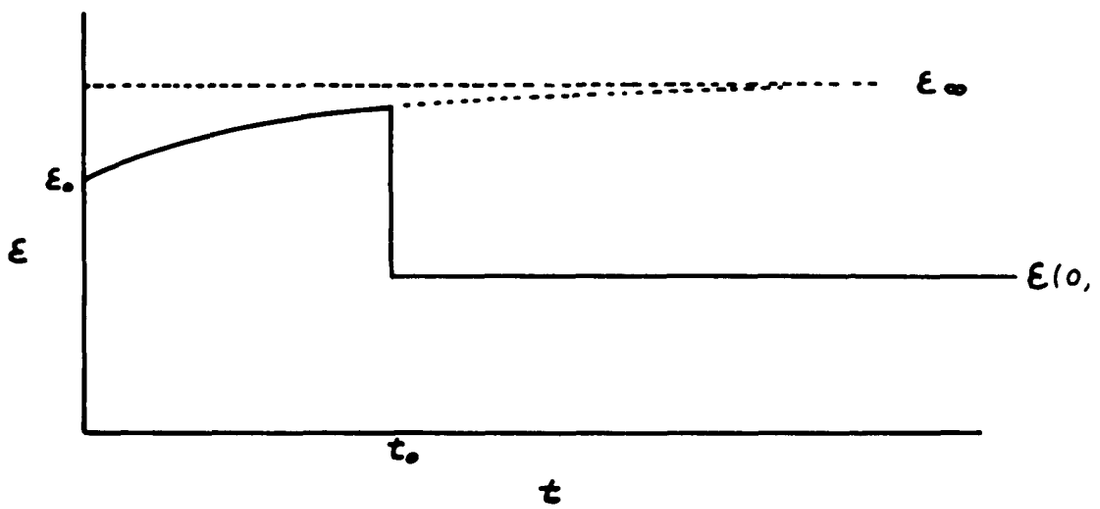

STRESS AND STRAIN AT X = 0

FIGURE IX

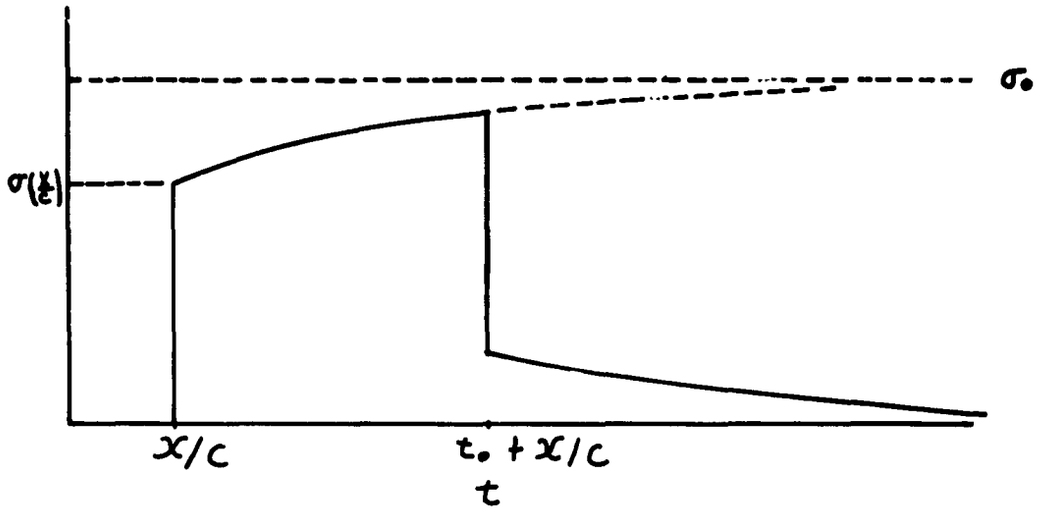

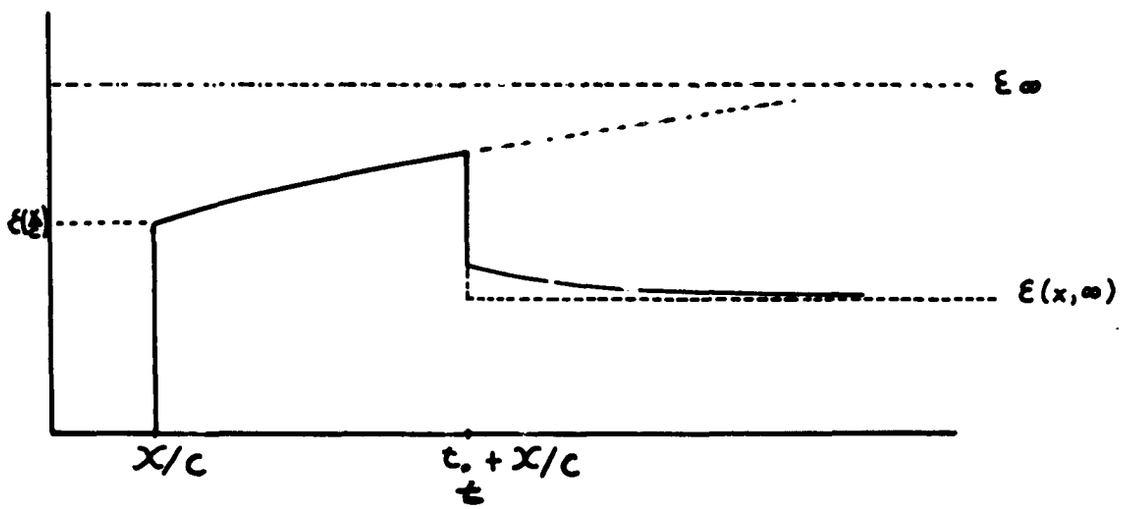

STRESS AND STRAIN AT $0 < X < X_p$

FIGURE X

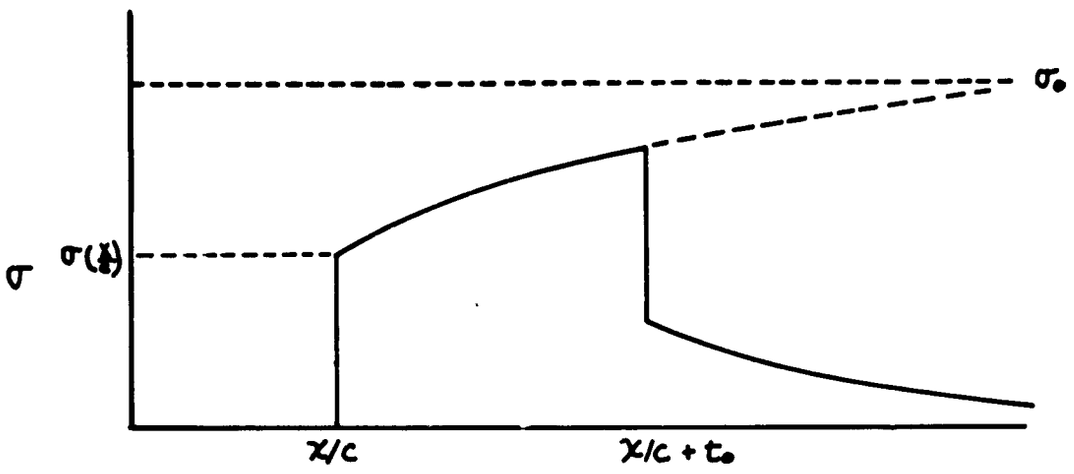

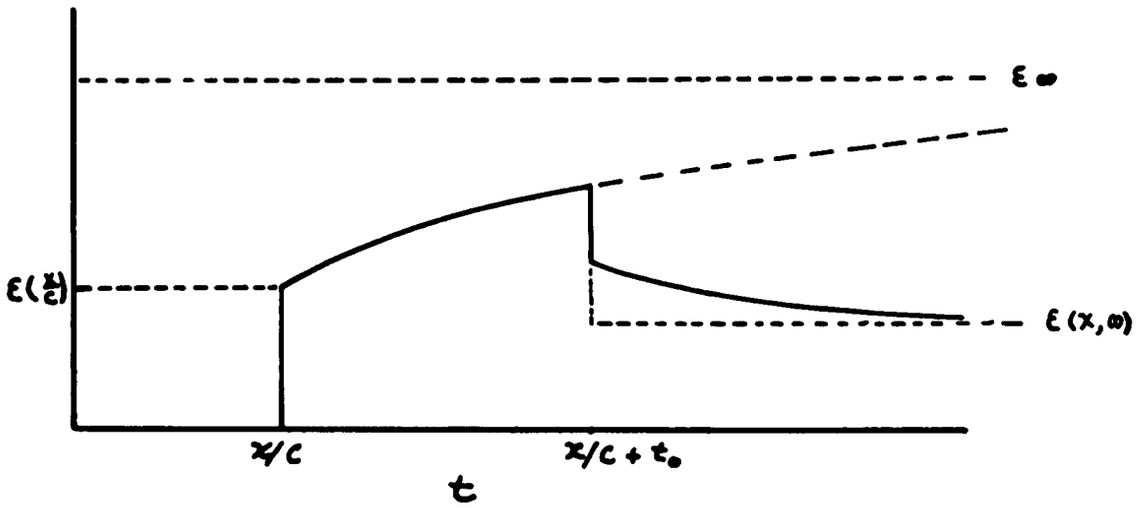

STRESS AND STRAIN AT $X = X_p$

FIGURE XI

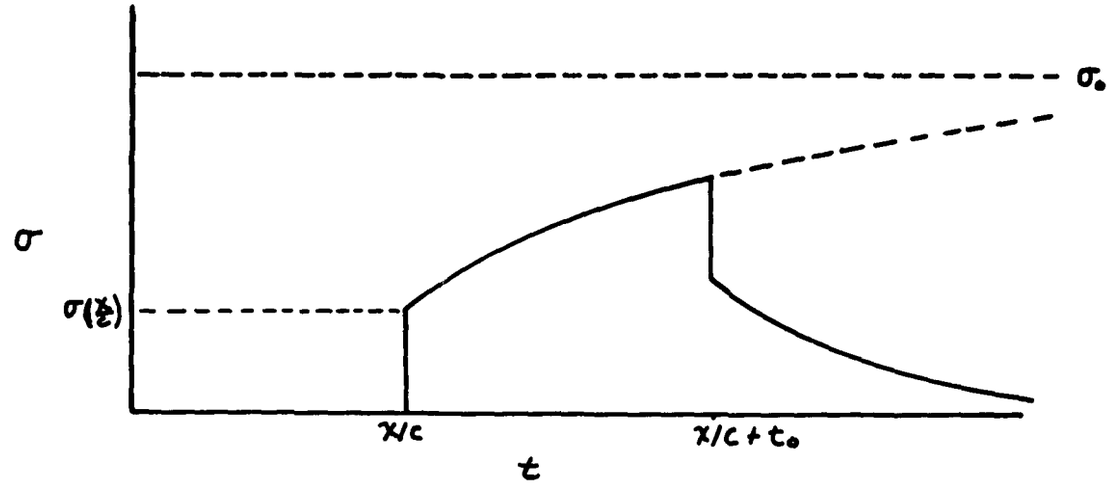

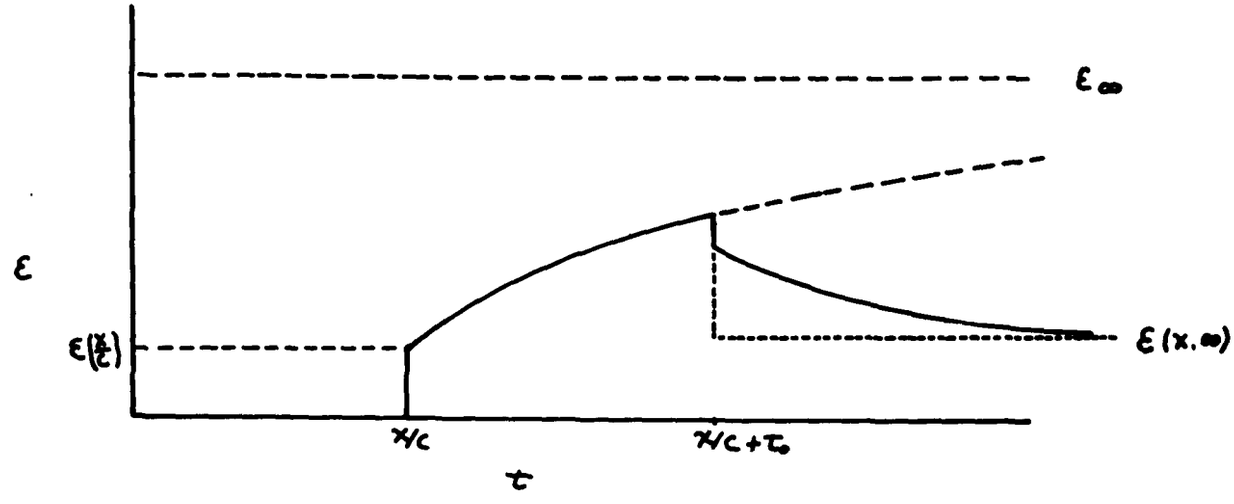

STRESS AND STRAIN AT $X_p < X < X_{ol}$

FIGURE XII

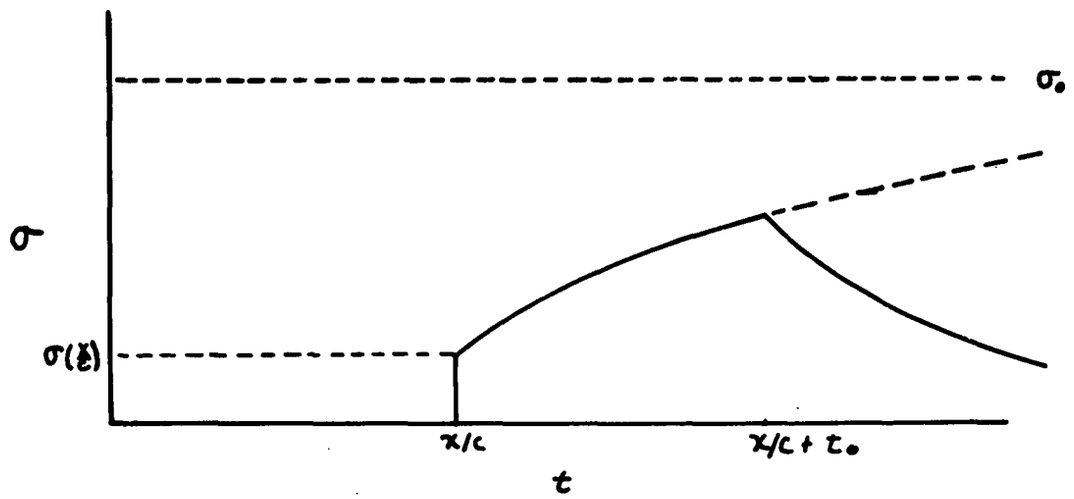

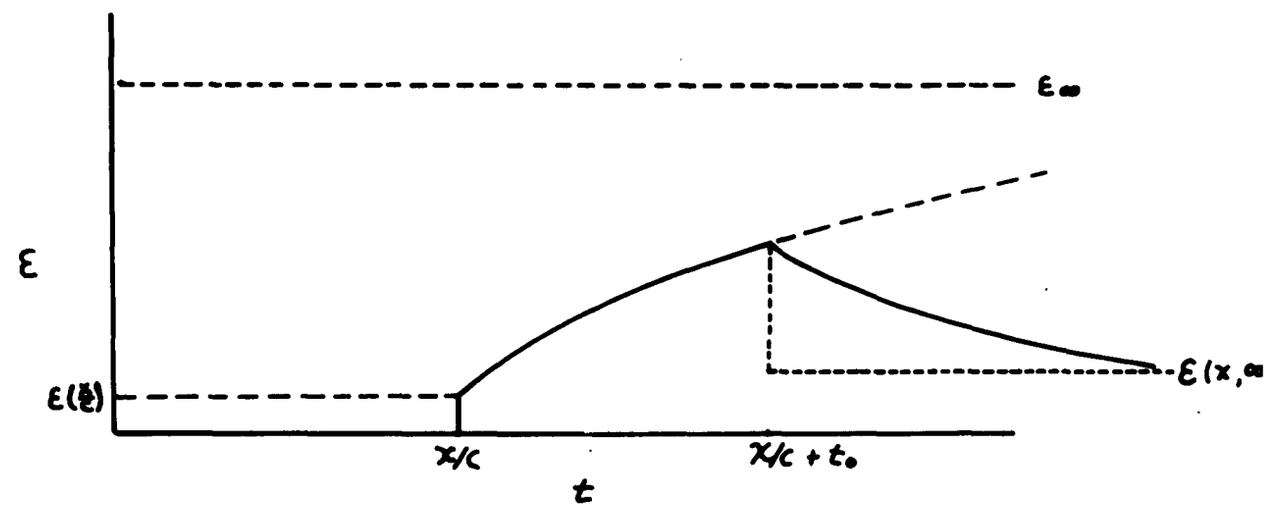

STRESS AND STRAIN AT $X=X_0$,

FIGURE XIII

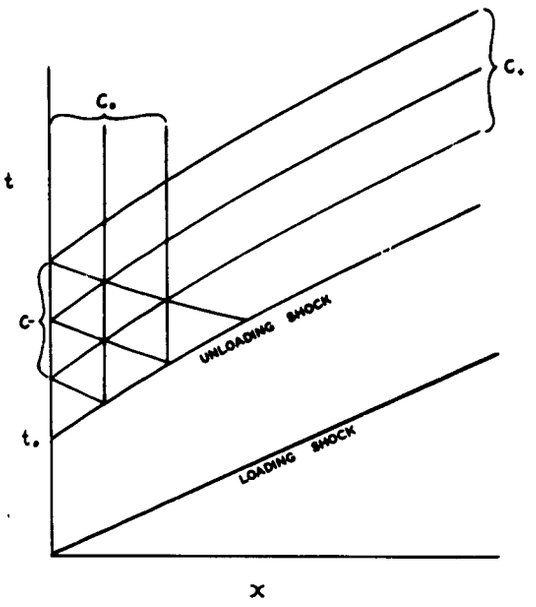

FIGURE XIV

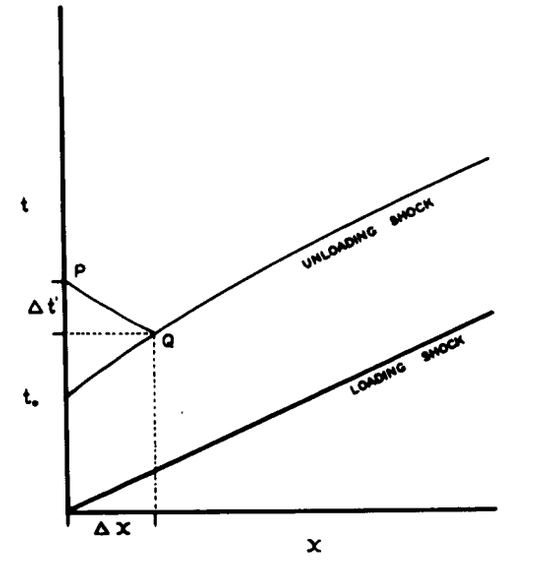

FIGURE XV

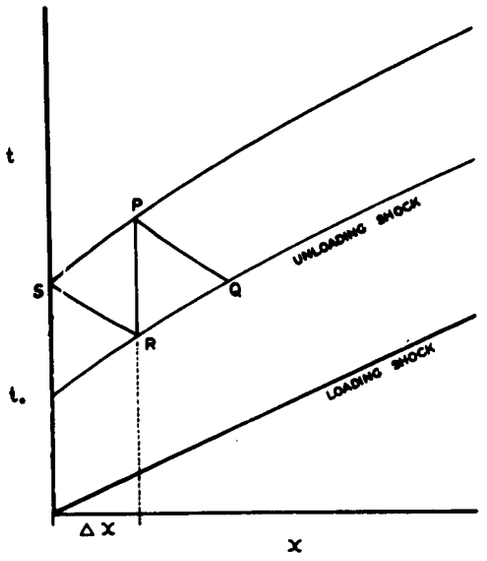

FIGURE XVI

DISTRIBUTION LIST

for

TECHNICAL AND FINAL REPORTS

Rensselaer Polytechnic Institute
Contract No. DA-30-115-509-ORD-1009

No. of Copies	Organization
1	Chief of Ordnance Department of the Army Washington 25, D. C. Attn: ORDTB - Bal Sec
1	Commanding Officer Diamond Ordnance Fuze Laboratory Washington 25, D. C. Attn: ORDTL-012
10	Director Armed Services Technical Information Agency Arlington Hall Station Arlington 12, Virginia Attn: TIPCR
6	British Joint Services Mission 1800 K Street, N. W. Washington 25, D. C. Attn: Reports Officer
3	Canadian Army Staff 2450 Massachusetts Avenue Washington 8, D. C.
2	Chief, Bureau of Naval Weapons Navy Department Washington 25, D. C. Attn: RRE
2	Chief of Naval Research Department of the Navy Washington 25, D. C. Attn: Code 118
1	Commanding Officer Naval Proving Ground Dahlgren, Virginia
2	Commander Naval Ordnance Laboratory White Oak Silver Spring, Maryland Attn. Mr. J. F. Moulton, Jr.
2	Director Naval Research Laboratory Anacostia Station Washington 20, D. C.
1	Officer in Charge Naval Civil Engineering Research & Evaluation Lab. Naval Station Port Hueneme, California Attn: Mr. J. Algood
1	Chief, Bureau of Yard and Docks Department of the Navy Washington 25, D. C. Attn: Cmdr. Saunders
1	Chief of Naval Operations Department of the Navy Washington 25, D. C. Attn: Op-36
1	Commanding Officer & Director David W. Taylor Model Basin Washington 7, D. C. Attn: Structural Mechanics Div.

Distribution List (Cont'd)

No. of Copies	Organization
1	Director Air University Library U. S. Air Force Maxwell Air Force Base Alabama
2	Commander Naval Ordnance Test Station China Lake, California Attn: Technical Library Editorial Section
1	Deputy Chief of Staff - Development Research & Development Directorate U. S. Air Force Washington 25, D. C. Attn: Major E. Lowery
2	Commanding General Special Weapons Command Kirtland Air Force Base Albuquerque, New Mexico Attn: Research & Development Col. P. L. Huie Dr. George Young
1	Commander Air Proving Ground Center Eglin Air Force Base Florida Attn: PGTRI
1	Commander Air Force Cambridge Research Center L. G. Hanscom Field Bedford, Massachusetts Attn: Geophysical Research Library
1	Commanding General Field Command Defense Atomic Support Agency P. O. Box 5100 Albuquerque, New Mexico
1	U. S. Atomic Energy Com. Military Applications Div. 1901 Constitution Ave., N. W. Washington 25, D. C.
1	Bureau of Mines, Chief Washington 25, D. C.
1	Commander Air Research Development Command U. S. Air Force Andrews Air Force Base Washington 25, D. C.
1	Deputy Chief of Staff Operations U. S. Air Force Washington 25, D. C. Attn: Asst. for Atomic Energy - AFOAT
1	Johns Hopkins University Operations Research Office 6935 Arlington Road Bethesda 14, Maryland
1	Commanding General U. S. Army Chemical Warfare Laboratories Army Chemical Center, Maryland
1	Commanding Officer Watertown Arsenal Watertown 72, Massachusetts Attn: Laboratory
1	Commanding General Frankford Arsenal Philadelphia 37, Pa. Attn: Pitman-Dunn Lab. Library Branch, C270, Bldg. 40

Distribution List (Cont'd)

No of Copies	Organization
2	Chief of Engineers Department of the Army Washington 25, D. C. Attn: Maj. Maurice K. Kurtz Mr. Martin Kirkpatrick
1	Commanding Officer Picatinny Arsenal Dover, New Jersey Attn: Mr. Joseph Hershkowitz
5	Director Defense Atomic Support Agency Department of Defense Washington 25, D. C. Attn: Mr. John Lewis
1	Director, Army Research Office Arlington Hall Station Arlington, Virginia Attn: Geophysics Branch
1	Executive Secretary Military Liaison Committee to the Atomic Energy Commission 1901 Constitution Avenue, N.W. Washington, D. C.
3	Director Waterways Experiment Station Box 631 Vicksburgh, Mississippi Attn: Mr. G. L. Arbuthnot Mr. William Flathau Mr. Robert Cunny
2	Los Alamos Scientific Laboratory P. O. Box 1663 Los Alamos, New Mexico Attn: Dr. Fred Reines
1	Applied Physics Laboratory Johns Hopkins University 8621 Georgia Avenue Silver Spring, Maryland
1	Armour Research Foundation Illinois Institute of Technology Center Chicago 16, Illinois Attn: Dr. T. H. Schiffman
1	RAND Corporation 1700 Main Street Santa Monica, California Attn: Dr. Brode
1	Sandia Corporation P. O. Box 5800 Albuquerque, New Mexico Attn: Physics Division Mr. W. R. Perret
1	Mr. Kenneth Kaplan Broadview Research Corp. 1811 Trousdale Drive Burlingame, California
1	Professor J. Neils Thompson Civil Engineering Dept. University of Texas Austin 12, Texas
1	Commanding Officer Army Research Office Box CM, Duke Station Durham, North Carolina
1	Stanford Research Institute Menlo Park, California Attn: Mr. F. Sauer
1	Dr. Robert V. Whitman Mass. Institute of Technology Cambridge 39, Massachusetts
1	Dr. Walter Bleakney Princeton University Princeton, New Jersey

Distribution List (Cont'd)

No of Copies	Organization
1	Dr. N. M. Newmark 111 Talbot Laboratory University of Illinois Urbana, Illinois
1	Dr. Otto LaPorte Engineering Research Institute University of Michigan Ann Arbor, Michigan
1	Engineering Research & Development Laboratory Fort Belvoir, Virginia Attn: Dr. T. G. Walsh
1	Dr. Leonard Obert Applied Physics Division U. S. Bureau of Mines College Park 1, Maryland
1	Lawrence Radiation Laboratory Livermore, California Attn: Dr. R. G. Preston
2	Commander Air Force Ballistic Missile Div. Air Force Research & Development Command Washington 25, D. C. Attn: Capt. W. E. Fluhr
1	Director Advanced Research Projects Agency Washington 25, D. C. Attn: Mr. Theodore George
1	Chief of Research & Development Department of the Army Washington 25, D. C. Attn: Lt. Col. Conarty Major Tyler
1	University of New Mexico Albuquerque, New Mexico Att: Mr. Frank Janza KAFB Shock Tube Facility
1	Professor W. H. Gardner, Jr. College of Engineering Durham, North Carolina
1	V. M. Davis Mine Warfare Branch U. S. Army Engineering Research & Development Lab. Fort Belvoir, Virginia
1	Dr. John M. Davies Pioneering Research Div. Quartermaster Research & Engineering Laboratories Natick, Massachusetts
1	Commanding Officer ASD Wright Patterson A.F.B., Ohio
10	Commanding General U. S. Army Ordnance Aberdeen Proving Ground Aberdeen Proving Ground Maryland Attn: ORDBG-BRU-T Mr. B. Perkins Mr. A. A. Thompson
1	Office of Technical Services Department of Commerce Washington 25, D. C.
1	W. Zagieboylo Quartermaster Research & Engineering Laboratories Natick, Massachusetts
1	Mr. R. C. Bryant Atlantic Research Corp. Shirley Highway at Edsall Rd. Alexandria, Virginia
1	University of Michigan Institute of Science & Tech. Attn: VESIAC, T.W. Caless Box 618 Ann Arbor, Michigan